Optimizing performance for cooling electronic components using innovative heterogeneous materials

F. Salmon [a,*], H. Benisi Ghadim [b], A. Godin [c,d], D. Haillot [b], A. Veillere [e], D. Lacanette [a], M. Duquesne [c]

[a] Bordeaux INP, CNRS, Université de Bordeaux I2M, Bât A11, 351 Cours de la Libération, 33400 Talence, France
[b] École de Technologie Supérieure (ÉTS), Department of Mechanical Engineering, 1100 Notre-Dame St W, H3C 1K3 Montréal, Québec, Canada
[c] La Rochelle Université, LaSIE UMR CNRS 7356, Avenue Michel Crépeau, CEDEX 1, 17042 La Rochelle, France
[d] 4ev Lab, EDF R&D, CNRS, LaSIE, La Rochelle University, Avenue Michel Crépeau, CEDEX 1, 17042, La Rochelle, France
[e] CNRS, Université de Bordeaux, Bordeaux INP, ICMCB, UMR 5026, 33600, Pessac, France

HIGHLIGHTS

- A review of thermal management in mobile phones, laptops, and data centers is given.
- A review of metal additive manufacturing techniques for porous structures is provided.
- The proposed triply-periodic minimal surface maximizes the interface heat transfer.
- 3D fluid–structure simulations are run with free codes.
- The performance of seven metals and three phase change materials is simulated.

Keywords:
Electronic devices
Thermal management systems
Phase change materials
Triply periodic morphologies
Heat transfer
Architected porous structure

SUMMARY

The relentless advancement of electronic devices has led to increased power densities, resulting in thermal challenges that threaten device reliability. This study aims to address this issue through the development of innovative heterogeneous materials for cooling electronic components. We focus on phase change materials (PCMs) impregnated within architected porous structures fabricated using additive manufacturing technology and 3D printing techniques. The objective is to leverage numerical simulations and additive manufacturing technology to select suitable materials and optimize heat dissipation within these structures. A comprehensive literature review of existing thermal management systems (TMS) for electronic devices, including mobile phones, laptops, and data centres, is presented. This review establishes a foundation for understanding the significance of TMS and introduces the benefits of employing PCMs in electronic devices. To assess the impact of the structure materials, we have run numerical simulations involving stainless steel, silver, Inconel, aluminium, copper, titanium, and steel architected porous structures impregnated with palmitic acid as the PCM. The results demonstrate the superior heat dissipation of silver, copper, and aluminium porous structures, attributed to their higher thermal diffusivities. Other simulations explore PCMs with higher melting temperatures and latent heat capacities, considering specific application parameters like mobile phones and laptops. By integrating three organic PCMs (Myristic acid, Palmitic acid, and Stearic acid) within architected matrices, it offers a promising solution in the choice of PCMs to the challenges posed by high power densities in electronics. This approach deepens our understanding of the melting process and allows the optimization of heat transfer within architected structures.

* Corresponding author.
E-mail address: fabien.salmon@bordeaux-inp.fr (F. Salmon).

https://doi.org/10.1016/j.apenergy.2024.122983

Nomenclature

List of symbols

T	Temperature (K)
c_p	Specific heat at constant pressure ($J.\ kg^{-1}.K^{-1}$)
ΔHf	Heat of fusion ($J.\ kg^{-1}$)
ρ	Density ($kg.m^{-3}$)
λ	Thermal conductivity ($W.m^{-1}.K^{-1}$)
μ	Dynamic viscosity ($Pa.\ s^{-1}$)

Subscripts

m	Melting

Acronyms

PCM	Phase Change Material
TMS	Thermal Management Systems

1. Introduction

The reliability of electronic devices is paramount to their success in the modern world. These devices are designed to perform specific functions accurately and precisely while maintaining safe and secure operations. Recent advancements in the fields of electronics and telecommunications have rapidly propelled the development of electronic devices, culminating in notable enhancements in their energy efficiency, processing speed, portability, and compactness. Therefore, in response to the growing demand for high-performance electronic devices, manufacturers have made efforts to increase the compactness of their products over the past few decades. As a result, the power density of electronic components has steadily risen.

Commercial processors, for example, have achieved power density values in excess of 100 $W.cm^{-2}$ [1,2]. The increase in power densities leads to the formation of thermal hotspots with values ranging from 0.1 to 1 $kW.cm^{-2}$, which can cause significant temperature fluctuations and exceed the recommended temperature thresholds for electronic components [3]. The significant temperature variations can cause thermal and mechanical stresses, which puts fast switching frequency equipment at particularly high risk. The reliability and safety of electronic components can be impacted if these temperature changes are not managed [4]. Approximately 55% of electronic devices failure is caused by high temperatures [5]. Consequently, it is crucial to develop effective thermal management systems (TMS) that can efficiently dissipate the heat generated by electronic devices. This is necessary to prevent thermal and mechanical strains, ensure component safety, and enhance reliability. These TMS must be capable of managing thermal transients resulting from high-frequency operating cycles, minimizing the formation of hotspots, and maintaining temperatures within acceptable limits [6].

Since efficient cooling of electronic components continues to be a major challenge in this industry, thermal management utilizing phase change materials (PCMs) has attracted substantial interest within the electronics community [7]. PCMs are gaining popularity in a variety of fields related to energy management. The use of these materials is expanding and changing as a result of present and future energy concerns. In particular, PCM applications that address energy-related issues are developing. Notably, there is a lot of interest in thermal energy storage, particularly when it comes to renewable energy sources [8]. Nevertheless, PCMs are hindered by their low thermal conductivity, which poses a significant limitation for TMS.

Numerous techniques aimed at enhancing the thermal conductivity and performance of PCMs have been explored and suggested. A comprehensive overview of diverse approaches to augment the thermal conductivity of low-conductivity PCMs is provided by Al-Omari et al. [9] . An innovative approach involves the impregnation of PCMs into architected matrices, which simultaneously addresses the concern of leakage in composite PCMs. However, certain challenges [10,11] such as intricate geometries, material wastage, precision, and tolerance are associated with the manufacturing of these structures using conventional methods like milling, shearing, drilling, casting, and forming.

To overcome these obstacles additive manufacturing technology can be employed. The advent of additive manufacturing technology, often referred to as three-dimensional (3D) printing, has eliminated manufacturing constraints, enabling the seamless fabrication of structures of any complexity. In the field of additively manufacturable materials, periodic cellular materials, particularly triply periodic morphologies, have drawn a lot of attention. These structures have found application in a diverse range of fields [12]. In order to utilize additive manufacturing technology for the production of architected porous structures, the selection of appropriate materials is essential. To streamline the process and save both time and costs, numerical simulations can be employed as an alternative to physically manufacturing the structures.

Hence, this study employs numerical simulations to aid in the selection of the most appropriate materials (PCM and metal) for the production of innovative architected structures. Utilizing a previously established computational framework [13], which incorporates sophisticated software tools such as OpenFOAM, CalculiX, and preCICE, a comprehensive series of simulations are conducted. In these simulations, seven distinct metals are considered as potential candidates for the architected porous structure. Subsequently, a numerical comparison is undertaken, focusing on the performance of three different PCMs. Notably, throughout these comparative analyses, the structural material of the porous framework remained consistent. This approach allowed for a rigorous evaluation of how various PCMs interacted with the same structural material, shedding light on their respective thermal characteristics and suitability for specific applications.

In this paper, we initiate by presenting a comprehensive review of TMS across diverse devices, including mobile phones, laptops, and data centres. In particular, the energy released by each electronic device, necessitating thermal management, is detailed and the most used TMSs to avoid overheating and failures are reviewed. Furthermore, this section delves into a comprehensive exploration of metal additive manufacturing techniques, as well as the meticulous selection of both metals and PCMs tailored to specific applications. Section 3 is dedicated to elucidating the methodology employed for testing the thermal performance associated to each considered material (PCM and metal). As the numerical modelling has previously been published [13], the mathematical structure is not detailed here, but only the general framework. The properties of the metals and the PCMs used in the simulations are provided in this section. Finally, the last section concerns the simulation results and engages in a discussion pertaining to the selection of suitable materials. The temporal evolutions of the PCM and metal temperatures, the associated heating rates and the liquid fractions of PCM are presented for the materials tested. Based on the numerical results, we are able to predict the thermal behaviour of the TMS and rank the materials. We also discuss on which couple PCM/metal to use depending on the application.

2. Literature review

TMS have numerous applications, including electric vehicles, mobile phones, laptops, data centres, and aircraft. Although all of these applications rely on TMS for their efficient operation, there exists a discrepancy in the amount of research conducted on them. While some have been extensively researched, others have received less attention. Electric vehicles and aircraft are two such applications that have been thoroughly investigated with regard to their TMS. A considerable amount of literature is available on the design and optimization of TMS for electric vehicles [14–18] and aircraft [19–24]. While these applications rely on TMS for their efficient operation, our study opts to concentrate on

specific areas with a smaller footprint such as mobile phones, laptops, and data centres, aiming for a more focused analysis.

2.1. Applications of TMS

2.1.1. Mobile phones

The rapid advancement of microelectronic technology and the telecommunications industry has produced numerous electronic devices, particularly ultra-slim mobile devices such as smartphones and tablets. Due to the limited availability of heat dissipation area, high-power electronic chips with high heat flux have been developed. The power consumption of smartphone processors has been increasing steadily in recent years [25].

Qualcomm Snapdragon, one of the most successful smartphone processors, exhibits full-load power consumption of 9–10 W [26]. It is widely accepted that power efficiency decreases when the temperature of a mobile phone's processor exceeds a specified limit of 50 °C [27]. Different types of TMS have been developed to dissipate heat efficiently from mobile phones. The most commonly used TMS are flat heat pipes [28–33] and ultrathin vapor chambers [34,35]. Based on recent studies, flat heat pipes are capable of maintaining the temperature of heat sources in the range of 80–109 °C under the heat flux range of 1.60–8.89 $W.cm^{-2}$, as reported by J. Li et al. [28], Sun et al. [30], Domiciano et al. [29], and Shioga et al. [32]. According to Chen et al. [34] and Huang et al. [35] research, ultra-thin vapor chambers have demonstrated the ability to maintain heat source temperatures in the range of 59–60 °C under a heat flux range of 2.89–4.44 $W.cm^{-2}$. While heat pipes and vapor chambers are commonly used as TMS for mobile phones, neither of these techniques can maintain the temperature of smartphone processors below 50 °C.

2.1.2. Laptops

Laptops have become powerful despite their small size due to integrated circuit packages that incorporate the CPU. However, their increased processing speeds in response to consumer demands have led to thermal issues that may compromise their functionality and stability [36]. Therefore, effective thermal management is crucial for the optimal performance of laptops, which face challenges in maintaining internal and surface temperatures within operational ranges of 85 °C and 40 °C, respectively [37].

The power consumption of a CPU is also a crucial factor that impacts a laptop's TMS, with Intel stating that its processors have a maximum power consumption of 160 W [38]. The most commonly used TMS methods are heat pipes and heat sinks, often complemented by fans. In a study by Zhao et al. [39], the effectiveness of a loop heat pipe utilizing nitrogen as the working fluid was assessed. The results indicated that the TMS was capable of sustaining the temperature of the heat source at 95 °C when the maximum heat flux applied was 1.67 $W.cm^{-2}$. Tian et al. [40] investigated the effectiveness of utilizing a combination of heat pipes and heat sinks for managing the temperature of small electronic devices such as laptops. Their findings indicate that this approach was capable of maintaining the heat source temperature at 100 °C even when subjected to a maximum heat flux of 30 $W.cm^{-2}$. The use of a fan for heat dissipation is a common technique in thermal management, along with heat pipes and heat sinks. A study by R. Singh et al. [41] showed that using a fan alongside a heat pipe and heat sink can maintain the CPU temperature at 85 °C with a maximum heat flux of 10 $W.cm^{-2}$. Lim et al. [42] and Wang et al. [43] have investigated effective cooling techniques for maintaining CPU temperature below the maximum acceptable temperature of 85 °C, including the combination of boiling-driven heat spreader with cold plates and vapor chamber with heat sink and fan.

Although the use of fans and cold plates can improve the performance of TMS, they can be distracting because of their noise and consume more power when running continuously. A potential solution to tackle this problem is to utilize conductive porous structure impregnated with PCMs into TMS, an area that has not received much research attention to date.

2.1.3. Data centres

The rapid growth of data centres in recent years has led to a significant increase in their power consumption, accounting for around 2.0% of the total energy consumed worldwide, which currently amounts to approximately 416 billion kWh per year [44]. To ensure the proper functioning and longevity of data centre equipment, effective thermal management systems are crucial. This is particularly important considering the projected increase in power density in data centres, expected to rise from 6 to 8 kW per rack to 50 kW per rack by 2025. Additionally, the power consumption of a single CPU may potentially exceed 250 to 300 W [45]. The safe and efficient operation of processing units requires that their temperature does not exceed a certain limit, typically considered as 85 °C in electronics thermal management research [45,46]. Therefore, it is imperative to explore innovative methods for enhancing cooling efficiency and reducing cooling power consumption to minimize energy consumption and emissions in green data centres.

Many studies and initiatives have been conducted to develop new cooling technologies and increase cooling effectiveness in data centres. Loop heat pipes have emerged as a widely used cooling technique. In recent studies by Zhou et al. [47] and Li et al. [48], the efficacy of loop heat pipes with water as the working fluid in data centres was investigated through experimental studies. Results demonstrated that their proposed cooling techniques were successful in maintaining the temperature of the heating source at 85 °C when the maximum heat flux was 8.40 $W.cm^{-2}$ and 25 $W.cm^{-2}$, respectively. Cooling plate [49] is another effective technique to maintain CPU temperature below maximum acceptable temperature in data centres. Xue et al. [45] and Cataldo et al. [50] conducted research on the combination of loop heat pipe and water cooler for cooling applications. Their proposed cooling methods were effective in maintaining the temperature of the heating source at 68 °C and 45 °C, respectively, when the maximum heat flux was 8.44 $W.cm^{-2}$ and 10.60 $W.cm^{-2}$.

2.2. Role of TMS in selected applications

With the rapid progress of technology, the demand for mobile phones, laptops, and data centres has surged, leading to higher power densities and increased heat generation. These devices face significant thermal challenges due to their compact designs, powerful processors, and continuous operation. As a result, efficient thermal management plays a crucial role in preventing performance degradation, component failure, potential safety hazards, and ensuring optimal operation and longevity of these devices. One of the primary challenges in implementing TMS in mobile phones and laptops, is the limited available space. These devices are becoming increasingly compact, leaving limited room for incorporating sophisticated cooling systems. Extensive experimental and mathematical investigations have been conducted to explore the potential of PCMs in serving as an alternative solution for achieving enhanced and uniform cooling in electronic devices [13,51]. During the process of phase change from solid to liquid or vice versa, the PCMs can effectively absorb and release a significant amount of latent heat.

However, there are several issues with PCM cooling, including limited thermal conductivity and leakage [52]. To fully leverage the benefits of PCMs in TMS, an additional challenge lies in the selection of suitable materials with high thermal conductivity, a critical factor for efficient heat dissipation. A recent approach to improve the thermal conductivity of PCMs involves embedding them within architected matrices featuring triply periodic morphologies like the gyroid structure. These morphologies are adept at optimizing the thermal pathway within the impregnated PCMs. As an example, integrating the primitive aluminium alloy structure with PCM resulted in an effective thermal

conductivity of 11.70 $W.m^{-1}.K^{-1}$, which is 58.5 times greater than the thermal conductivity of the pure PCM (0.20 $W.m^{-1}.K^{-1}$) [53]. These kinds of architected matrices have been extensively investigated for applications in structural and thermo-mechanical domains. However, there exists a research gap when it comes to utilizing these matrices in conjunction with PCMs for TMS in electronic devices. Examples of some triply periodic morphologies are presented in Fig. 1.

In comparison to conventional strut-based topologies and metal foam cells, triply periodic structures have consistently shown improved performance in a variety of applications. The prospective uses of these structures for heat transfer have not been fully investigated, despite their remarkable performance in a variety of applications. Al-Ketan et al. [54] performed steady-state simulations with air as the working fluid to investigate the heat transfer properties of triply periodic structure-based heat sinks. According to their research, the porosity and particular design of the architecture had an impact on the convective heat transfer efficiency of the heat sinks. When combined with PCMs to create composite materials, these architected structures hold the potential for enhanced heat transfer performance. This is due to their proven success in various applications and their higher surface area density compared to traditional structures [12].

Triply periodic structures can be effectively manufactured using highly thermally conductive materials such as copper. However, the utilization of conventional manufacturing techniques like milling, shearing, drilling, casting, and forming to create intricate structures faces a multitude of challenges. These subtractive techniques involve material removal to achieve the desired geometry. A number of challenges arise from employing these conventional manufacturing methods for crafting complex structures. Firstly, design freedom is constrained due to the limitations imposed by the available tools and processes. Furthermore, these techniques necessitate material removal to attain the desired morphology, resulting in material wastage, especially when dealing with intricate geometries. Additionally, the process of incremental material removal to achieve the final shape is inherently time-consuming. The complexity and repetitive nature of triply periodic structures demand meticulous material removal efforts to ensure precision and prevent errors. Additive manufacturing technology has eliminated industrial limitations and made it possible to easily fabricate any type of construction, regardless of its complexity. The recent advancements in this technology provide us with the means to address difficulties that were previously encountered when employing conventional manufacturing approaches.

To illustrate, the method of layer-by-layer material deposition in these processes affords meticulous oversight over both geometry and material allocation. This capability proves instrumental in the fabrication of intricate structures, such as the gyroid. Additional information regarding additive manufacturing techniques will be covered in the following section.

2.3. Metal additive manufacturing

In the current era of additive manufacturing, advanced technologies have emerged for the production of a diverse range of products. These technologies encompass the use of various materials, including metals, polymers, ceramics, and composite materials. Among these, it can be argued that metal additive manufacturing (MAM) stands out as having a profound impact across a multitude of industries such as electronic [55]. Significant progress in electronic devices has been achieved through revolutionary technologies, particularly the development of efficient, compact and lightweight cooling systems. This progress is driven by continuous efforts to design heat exchangers that strike a balance between efficiency and compactness, marked by their lightweight build and minimized material consumption.

In accordance with ASTM/ISO 52900:2017 [56], MAM processes are broadly sorted into four main categories, which encompass material extrusion (ME), binder jetting (BJ), powder bed fusion (PBF), and directed energy deposition (DED). A diverse array of materials has been specifically engineered for MAM. These encompass copper alloys, aluminium alloys, stainless steel, nickel-based superalloys, titanium alloys, cobalt alloys, and refractory alloys [57]. Powder-based materials represent the predominant choice, although in certain instances, wire materials are also employed. These materials are subjected to melting or sintering processes, in order to induce solidification in both cases. Energy sources such as lasers or electron beam are used for the

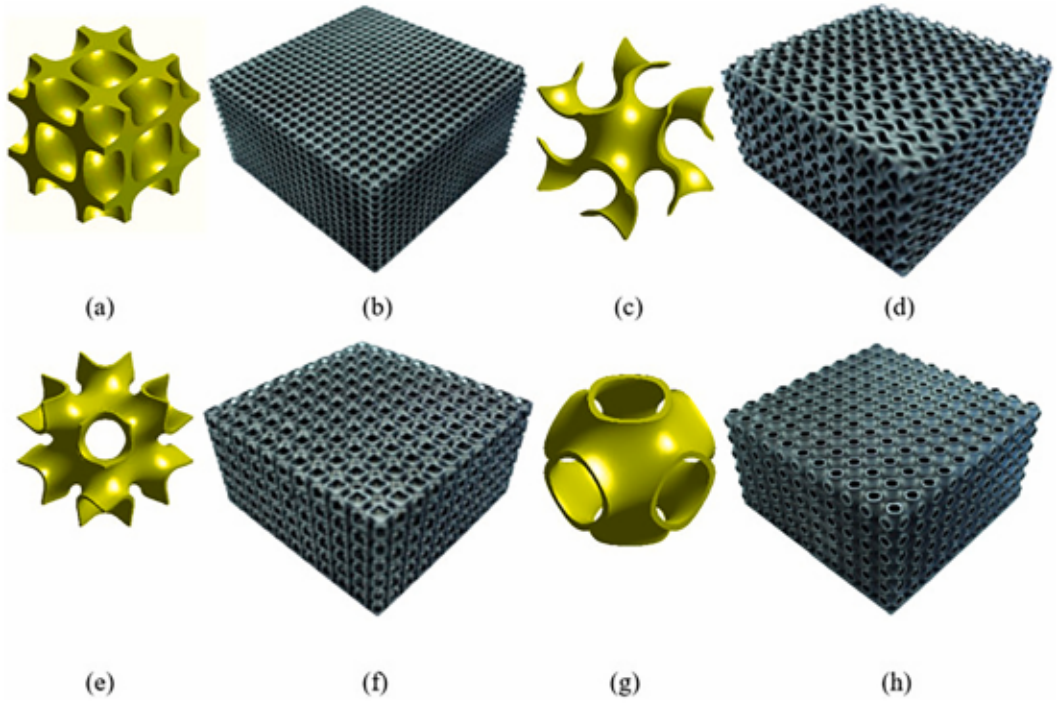

Fig. 1. CAD models for unit cells and 3D Printed Triply periodic surfaces lattices for (a)&(b) Diamond, (c)&(d) Gyroid, (e)&(f) IWP, and (g)&(h) Primitive [12].

densification [58].

ME is distinguished by the process of extruding material to fabricate a 3D component. In contrast with other MAM processes that utilize unconsolidated metal powders, ME machines employ pliable feedstocks. These feedstocks consist of metallic powders enveloped within polymer matrices, which act as an integral binding system [59]. A typical ME machine is comprised of essential components, including a build platform, a print head, and a metal filament.

BJ works in a similar way to how ink is applied to paper. However, instead of functioning solely in two dimensions (x, y), this process leverages the third dimension (z) to fabricate a solid component. In this process, metallic powder particles bond together through the presence of a liquid binder. It is worth noting that the printing is conventionally conducted at room temperature [60]. Unlike other MAM processes reliant on heat sources, this approach helps to eliminate thermally induced imperfections such as undesirable grain growth and distortion [61]. It is important to note that for both ME and BJ techniques, the production of metal parts involves a post-printing process. The process includes a debinding step to eliminate polymers used for binders after which the metal parts are densified.

PBF is the process of applying thermal heat to melt or sinter metal particles, resulting in a solid product. PBF methods vary but share common characteristics, including an inert build chamber to prevent metal oxidation, a heat source to fuse metal powder particles, a fusion control mechanism, and a layer-by-layer deposition and smoothing process [55]. The primary difference is in the energy source used, which is often lasers or electron beams.

DED is a manufacturing process that employs a concentrated thermal energy from the heat source to liquefy material while it is being dispensed through a nozzle, akin to the fundamentals of welding. DED is generally used to fabricate parts that are almost net-shaped and to repair or improve upon existing components. It constitutes approximately 16% of the overall MAM market [62]. DED processes commonly utilize four distinct sources of thermal energy: plasma laser, electron beam, electric arc, and laser beam [55].

A review study conducted by Kaur and Singh [63] compared additively manufactured heat exchangers to conventional ones. They highlighted the substantial impact of surface roughness, particularly in heat exchangers produced through PBF techniques. Additively manufactured heat exchangers exhibited surface roughness levels up to ten times higher than their conventionally manufactured counterparts. This heightened surface roughness primarily influenced pressure drop rather than heat transfer efficiency. Therefore, for the design and evaluation of such heat exchangers it is essential to take into account accurate measurements and a coherent documentation of surface roughness and associated process parameters. In another research, S.K. Dhinesh et al. [64] conducted a comprehensive review study on the role of additive manufacturing in electronic devices. Research findings underscore the substantial cost reductions achieved through additive manufacturing to nearly a 50% reduction in final production costs compared to conventional manufacturing methods. However, it is vital to acknowledge that additive manufacturing is not without its challenges. Issues related to density, strength, accuracy, and surface finish have been recognized. Consequently, post-processing steps become imperative in refining additively manufactured components.

Selema et al. [65] conducted a comprehensive comparison of PBF, BJ, and DED technologies, evaluating their cost, speed and resolution, as well as quality and safety aspects . Within the domain of MAM, three primary cost determinants were identified: the expenses associated with the printing process, the procurement of raw materials, and the post-processing procedures. The material cost was considered the most significant one among them, particularly when the main print material was high-quality powder, as was the case in PBF. It was also crucial to include any secondary materials, such as the binders used in BJ. PBF incurred the highest cost due to its demand for small and spherical powder, which is costly to manufacture. This differs from BJ or powder DED, where the powder utilized is of lower quality and more affordable. The lowest costs were associated with the wire-based MAM techniques, except for wire DED, which requires expensive postprocessing, resulting in an overall cost almost in line with powder DED, despite the relatively higher cost of powder. In terms of print speed and resolution, it was observed that powder-based systems typically excel in offering high resolution, albeit at slower printing speeds. BJ, however, emerges as an exception, as it allows for faster printing. Nevertheless, it necessitates a subsequent de-binding and sintering process. On the contrary, wire-based systems can achieve significantly higher printing speeds, reaching up to 10 $kg.h^{-1}$. However, this comes at the cost of lower resolution. In terms of safety and quality it was found out that because of the high surface area, wire-based techniques have superior quality and safety compared with powder metals that are more sensitive to environmental factors such as moisture and oxidation affecting component quality. In terms of safety, powders pose a greater fire risk compared to wires. Armstrong et al. [55] conducted a comprehensive review of MAM techniques. Their findings suggest that ME and PBF methods exhibit greater suitability for manufacturing metal components. One key factor contributing to this preference is the superior printing resolution offered by ME and PBF compared to DED and BJ methods. Additionally, among ME and PBF, the ME technique stands out for its cost-effectiveness, ease of use, and overall economic advantages. Although PBF currently stands as one of the most widely adopted technologies for printing metallic parts, it does present certain challenges due to the intricate melt pool mechanisms it involves. These challenges manifest as significant defects, including high surface roughness, porosity, and residual stress. Common drawbacks associated with both ME and PBF techniques include the necessity for support structures for overhanging or unsupported features and the requirement for post-processing to address issues related to poor surface finishes.

Surface imperfections and poor finish can significantly impact the performance of components manufactured using MAM. To address this issue, Maleki et al. [66] conducted a review focusing on various surface post-treatment methods for metal components produced through MAM techniques. Their study categorized these treatments into three main groups: mechanical, laser-based, and chemical treatments. The research revealed that the choice of treatment method is primarily influenced by factors such as surface quality, material characteristics, part geometry, and the intended function of the additively manufactured metal part. Mechanical and laser-based treatments were found to be particularly effective in enhancing the mechanical properties of additively manufactured metallic components. On the other hand, chemical surface treatments were identified as valuable for providing comprehensive surface treatment, including access to internal surfaces within complex and intricately designed parts. Consequently, for components wit complex geometries like lattice and mesh structures, chemical treatments demonstrated greater effectiveness compared to mechanical methods, which are often constrained by the part's geometry and dimensions.

2.4. Selection of materials

2.4.1. Metals

In order to effectively dissipate heat and maintain a device's overall performance, it is essential to use the right materials for metal heat exchangers in electronic devices. With the advent of numerical simulations, researchers have gained a powerful tool to compare and evaluate different metals for optimal material selection. This study employs numerical simulations in order to select the most suitable metals for manufacturing of the architected porous structure to be backfilled with PCM and to be utilized for cooling of electronics. One significant advantage of employing numerical simulations in the design of metal porous structure is the potential for cost optimization. 3D printing manufacturing processes often involve extensive trial and error approaches, resulting in high production costs. By utilizing numerical simulations, we can minimize the number of physical prototypes

required and select the most appropriate material combinations, significantly reducing manufacturing costs. Additionally, numerical simulation enables the selection of the most suitable materials for manufacturing the metal porous structures.

By considering various factors such as thermal conductivity and compatibility with the surrounding components, we can identify materials that enhance heat dissipation and improve overall system performance. This approach ensures that the selected materials are specifically tailored to meet the thermal management requirements of electronic devices. Durgam et al. [67] conducted a numerical investigation on advanced heat sink materials for the thermal management of electronics. They studied forced water convection in micro-channel heat sinks made of copper alloy (CuMo) with a thermal conductivity of 250 $W.m^{-1}.K^{-1}$, and aluminium alloy (Al6060) with a thermal conductivity of 209 $W.m^{-1}.K^{-1}$. The simulation was carried out using Ansys Fluent software, considering three different velocities (3, 5, and 7 $m.s^{-1}$) and a constant heat flux value of 8×10^5 $W.m^{-2}$. The results of the study demonstrated that the heat transfer coefficients of the copper alloy heat sink, at velocities of 3, 5, and 7 $m.s^{-1}$, were measured to be 1.4, 1.9, and 2.3 $W.m^{-2}.K^{-1}$, respectively. In comparison, the heat transfer coefficients of the aluminium alloy heat sink, under the same velocities, were determined to be 1.0, 1.6, and 1.8 $W.m^{-1}.K^{-1}$. In the investigated study, it was observed that copper alloy exhibits superior heat transfer performance compared to aluminium alloy across all examined flow velocities. However, it should be noted that when compared to aluminium alloy, copper alloy presents difficulties in terms of machining capability, greater cost, and increased weight. Consequently, considering these factors, aluminium alloy is generally favoured as the preferred heat sink material.

In another study, Muhammad et al. [68] conducted a comprehensive numerical simulation to examine the heat transfer capabilities of liquid metal-cooled mini-channels with various heat sink materials. The study employed gallium alloy (GaIn) as the coolant with a thermal conductivity of 39 $W.m^{-1}.K^{-1}$ as the coolant. Copper alloy, with a thermal conductivity of 391 $W.m^{-1}.K^{-1}$, as well as aluminium (237 $W.m^{-1}.K^{-1}$), tungsten (174 $W.m^{-1}.K^{-1}$), and silicon (148 $W.m^{-1}.K^{-1}$) were selected as the heat sink materials under investigation. To investigate the variations in heat dissipation capacity among the heat sink materials, a numerical calculation was performed to determine the maximum heat flux. The heat flux at the base of the heat sinks was gradually raised until the temperature of the heat sink's base reached 350 K. The findings revealed notable differences in the maximum heat flux achieved by various heat sink materials. Specifically, the copper heat sink exhibited the highest heat flux of 265 $W.cm^{-2}$, followed by aluminium at 211 $W.cm^{-2}$. Tungsten and silicon heat sinks demonstrated lower maximum heat flux values of 182 and 169 $W.cm^{-2}$, respectively.

Siahchehrehghadikolaei et al. [69] conducted a research study aimed at developing a 3D Computational Fluid Dynamics model to analyse the thermal performance of pin heat sinks used for CPU cooling. In their investigation, they employed various metals, including copper, nickel, and silver, to simulate the fin structure of the heat sink. Additionally, a nanofluid composed of graphene and water was utilized. The study's findings revealed that, when subjected to a heat flux of 100,000 $W.m^{-2}$, the silver heat sink outperformed both copper and nickel counterparts due to its superior thermal conductivity. Specifically, the attained minimum CPU temperatures were 77 °C, 82 °C, and 97 °C for the silver, copper, and nickel heat sinks, respectively. In another research, Zhang et al. [70] engineered a heat exchange system for nitrogen-to-air transfer, employing Inconel 718 with a thermal conductivity of 9.94 $W.m^{-1}.K^{-1}$ as the material of choice. The fabrication method used was laser powder bed fusion. Their research findings highlighted the remarkable potential of additive manufacturing for the production of compact and lightweight heat exchangers, particularly valuable in situations where limitations exist concerning spatial and weight constraints. As a result of their efforts, they successfully boosted heat transfer density by 25% in comparison to traditional fin heat exchangers, ultimately achieving a remarkable heat exchange rate of up to 2.78 kW. Additionally, they explored the applicability of this technology in the realm of microfluidics for the effective thermal management of electronic components.

Enhancing the heat dissipation capabilities of metals can be achieved by adding high thermal conductivity materials like graphene. This addition improves thermal conductivity while minimizing expansion coefficients, rendering it a vital material for effective thermal management applications. Chu et al. [71] achieved an impressive in-plane thermal conductivity of 525 $W.m^{-1}.K^{-1}$ in graphene/copper composites by incorporating 35% volume of graphene nanoplatelets. In another study Rojo and Darabi [72] conducted both experimental and computational research to assess the effectiveness of copper/carbon nanotube (CNT) micropillars in the thermal management of electronic devices. The outcomes of their studies indicated that the proposed copper/CNT combination, with a remarkable thermal conductivity of 704.2 $W.m^{-1}.K^{-1}$, exhibited impressive heat dissipation capabilities, effectively handling heat fluxes as high as 80 $W.cm^{-2}$. Furthermore, the highest temperature recorded at the substrate's surface during testing was a mere 38.5 °C, showcasing its efficient cooling performance. Similar to the previously examined research, this study draws the conclusion that while copper exhibits superior heat dissipation properties, factors such as cost and weight make aluminium a viable material choice for manufacturing metal porous structures.

2.4.2. Ceramics

In addition to metals, there has been significant progress in the evolution of ceramic materials for additive manufacturing techniques. Ceramics constitute a distinct category of materials known for their elevated thermo-chemical stability and high melting points. Their outstanding resistance to oxidation makes them suitable for deployment in demanding reactive settings, including gas turbines, heat exchangers, nozzles, and heat protection systems [73,74]. The potential of 3D architectures featuring porous channels alongside a high thermal conductive ceramic skeleton is substantial for various engineering and industrial applications, particularly in the realm of thermal management. It is mainly due to its low weight, as well as their ability to significantly improve heat transfer through effective conduction and convection mechanisms [75].

In the study conducted by Sarowar [76], an examination was carried out on the heat transfer characteristics of a mini-channel heat sink utilizing five distinct ceramic substrates. These substrates included aluminium nitride, beryllium oxide, hafnium diboride, titanium diboride, and zirconium diboride. The findings from the research clearly indicate that, in terms of performance, a heat sink constructed with aluminium nitride outperforms all other substrate materials. Cao et al. [77] conducted a numerical investigation to assess the impact of introducing beryllium oxide on the heat transfer efficiency of a heat exchanger with microchannels and fins. Their results demonstrated a notable enhancement, with the heat exchanger employing trapezoidal fins showing an approximately 219% increase in effectiveness compared to the device made of alumina, as reported in their research. In another research project, Sarowar [78] carried out an analysis to gauge the influence of three boron-based ultra-high-temperature ceramic materials (zirconium diboride, titanium diboride, and hafnium diboride) on the highest attainable temperature and thermal performance of a microchannel heat sink. The findings revealed that, under conditions where the heat flux was 3.6 $MW.m^{-2}$, none of the materials exceeded a maximum temperature of 82 °C. Additionally, the research indicated that, in comparison to zirconium diboride, both hafnium diboride and titanium diboride demonstrated more favourable characteristics as substrate materials.

It is evident that ceramics, in addition to metals, offer a compelling

choice when it comes to the manufacturing of heat exchangers for electronic devices. Their unique combination of high thermo-chemical stability, elevated melting points, and remarkable resistance to oxidation makes ceramics a valuable contender in the field of thermal management. These materials, characterized by their lightweight nature and the capacity to significantly enhance the heat transfer through efficient conduction and convection, hold immense promise for meeting the demanding thermal needs of modern electronic devices. Hence, considering ceramics alongside metals in the design and construction of heat exchangers provides engineers and researchers with a versatile toolkit to address the ever-evolving challenges of electronic device thermal management.

2.5. Phase change materials (PCMs)

The selection of an appropriate PCM for effectively managing the thermal aspects of electronic components involves a comprehensive assessment of several critical factors such as suitable melting temperature, high latent heat, high specific heat, high thermal conductivity, and thermal stability [79]. At the outset, careful consideration is given to the melting point of the PCM in relation to the temperature range that aligns with the specific application under scrutiny. Notably, it is imperative to align the PCM's melting point with the operational temperatures of the particular electronic component being studied. This is exemplified by the upper temperature limits that have been established as permissible for different components, with mobile phone processors restricted to 50 °C [34], and CPUs of laptops and data centres constrained to 85 °C [37].

In order to minimize the PCM quantity needed and optimize heat transfer efficiency, consequently leading to reduced charging and discharging durations, the pursuit of specific desirable characteristics becomes imperative. These characteristics encompass a higher latent heat per unit mass, elevated specific heat within the solid phase, and superior thermal conductivity. By prioritizing these attributes, the overall thermal management performance can be significantly enhanced, promoting efficient and effective heat dissipation processes [51]. PCMs can be classified into categories of organic, inorganic, and eutectic compositions. To incorporate PCMs into the TMS of electronic devices, compatibility with metals like copper is crucial. Organic PCMs, unlike inorganic PCMs, offer non-corrosive attributes, rendering them suitable for impregnation into metal structures to serve as composite PCMs in electronic device TMS applications.

Bianco et al. [51] conducted a comprehensive review aiming at identifying the most suitable PCMs for thermal management applications in electronic devices, including mobile phones and laptops. The study highlighted several PCM options, including fatty acids, paraffins, n-alkanes, hydrated salts, and liquid metals, based on their specific melting temperature ranges. Among these PCMs, liquid metals were found to offer the highest density while having the lowest latent heat of fusion. On the other hand, n-alkanes exhibited the highest latent heat of fusion. However, the relatively high cost associated with n-alkanes rendered them less suitable for PCM applications in electronic device thermal management. Salt hydrates were identified as having the potential to provide the desired melting temperature range. However, they came with certain drawbacks, including phase separation during the solid-to-liquid phase transition, supercooling, and incompatibility with materials such as stainless steel, aluminium, and copper. As a result, the study concluded that fatty acids and paraffin-based PCMs emerged as the most suitable choices. These options were preferred due to their absence of drawbacks commonly found in salt hydrates and their more cost-effective nature when compared to n-alkanes.

Within the category of organic PCMs, fatty acids are recognized for their impressive thermal stability [80]. Several well-investigated fatty acids encompass caprylic acid, capric acid, lauric acid, myristic acid, palmitic acid, and stearic acid [81]. In the context of PCM thermal properties, the melting temperature plays a pivotal role, particularly in the TMS of electronic devices. The melting temperatures of various fatty acids are provided in Table 1.

Table 1
Melting temperature of fatty acids.

Compound	Chemical formula	T_m (°C)	Ref
Caprylic acid	$C_8H_{16}O_2$	16	[82]
Capric acid	$C_{10}H_{20}O_2$	32	[82]
Lauric acid	$C_{12}H_{24}O_2$	44	[82]
Myristic acid	$C_{14}H_{28}O_2$	52	[82]
Palmitic acid	$C_{16}H_{32}O_2$	61	[83]
Stearic acid	$C_{18}H_{36}O_2$	70	[82]

As indicated in Table 1, fatty acids exhibit a broad spectrum of melting temperatures, which renders them advantageous for cooling electronic devices. As previously mentioned, these PCMs can be impregnated into architected thermal conductive porous structures to amplify the composite PCMs' thermal conductivity.

To assess the viability of the proposed innovative TMS, numerical simulations can be employed. A recent study was conducted by Salmon et al. [13], wherein they formulated a model to simulate conduction and convection heat transfer within both the PCM and the gyroid porous structure. Consequently, we employed this model to facilitate the selection of the most suitable metals for manufacturing our metal architected porous structures. Additionally, we will utilize the model to conduct further simulations aiming at identifying the optimal PCMs for TMS in electronic devices.

The reviewed literature underscores the critical role of thermal management systems (TMS) in a diverse array of applications, ranging from mobile phones and laptops to data centres. This review delves into the thermal challenges of mobile phones, laptops, and data centres, presenting an innovative approach to address the above-mentioned issues through architected porous structures impregnated with PCMs. The seamless connection between the literature review and the proposed methodology demonstrates the relevance and novelty of this study. By exploiting the potential of architected porous structures and PCMs, this research strives to pave the way for innovative solutions in electronic device thermal management.

3. Methodology

In this study, numerical simulations were conducted to investigate the heat dissipation capability of metallic porous architected structure. The conducted simulation is adopted from Salmon et al. [13], which plays a crucial role in enabling the selection of optimal materials for the fabrication of our metal porous structure, as well as identifying suitable PCM candidates. This model offers a sophisticated tool for investigating heat dissipation capabilities within architected metallic porous structures, thereby laying the groundwork for the subsequent endeavours undertaken in this study. The fluid-structure model is based on open-source software, OpenFOAM, which solves the equations governing the PCM, CalculiX, which manages the structural part, and preCICE, which handles the interface coupling between the two codes. This numerical modelling is described in detail in [13], where a validation on experimental data was presented.

The simulated structure was fabricated using different materials: steel, silver, aluminium, Inconel, stainless steel, copper, and titanium. The structure was impregnated with palmitic, myristic or stearic acid as PCM. In order to maximize the heat transfer exchange surface, the shape of the encapsulating structure is based on triply-periodic minimum surfaces [84], like in the simulations managed by Salmon et al. [13]. The gyroid structure is given by the implicit equation $cos(x)sin(y) + cos(y)sinx(z) + cos(z)sin(x) = 0.15$. The geometry of the porous architected structure used in the numerical simulations of this article is depicted in Fig. 2.

Furthermore, dimensions play a pivotal role in orchestrating

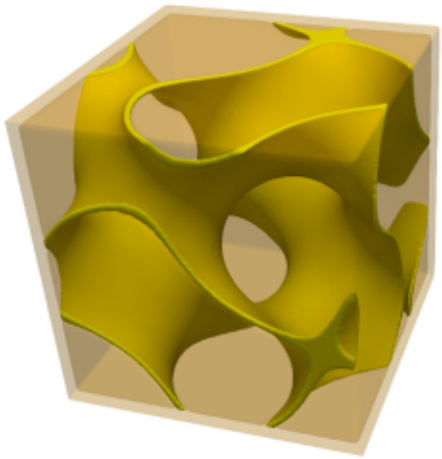

Fig. 2. The sections coloured in yellow, as well as the encompassing enclosure, possess a solid composition, whereas the remaining portion exhibits a liquid state [13]. (For interpretation of the references to colour in this figure legend, the reader is referred to the web version of this article.)

effective heat transfer mechanisms. The enclosing box, a central element of the study's simulation setup, exudes uniformity with a side length of 5 cm. This harmonized dimensionality serves as the canvas upon which the intricate interplay of heat dissipation unfolds.

Table 2 outlines the properties that have been taken into consideration for both PCMs and employed metals in the simulations. They correspond to the melting temperature T_m, the heat of fusion ΔH_f, the density ρ, the specific heat at constant pressure c_p, the thermal conductivity λ and the dynamic viscosity μ.

The thermal behaviour of the impregnated porous architected structure with PCM was simulated for each metallic structure and each PCM under a power supply of 30 W applied to the bottom face. Convective heat transfer with a coefficient of 5 $W.m^{-2}.K^{-1}$ and an outside temperature of 22 °C occurred on the other external faces of the box.

4. Results and discussion

4.1. Influence of the structure material

We present the results of simulations corresponding to porous architected structures crafted from seven distinct metals: steel, silver, aluminium, Inconel, stainless steel, copper, and titanium, all incorporating palmitic acid as a PCM. The core aim of the preliminary simulations is to scrutinize the correlation between time and temperature within the PCM/porous metal structures. This scrutiny aims to quantify the effectiveness of heat dissipation for each structure based on different metals. The outcomes of the simulation are presented in Fig. 3.

The PCM starts to melt at around 300 s in silver, copper and aluminium structures, as shown in Fig. 3b, with the fraction of liquid PCM increasing from this point. This can also be seen with the break in the slope of the average temperature in Fig. 3a, which is also visible in Fig. 3d presenting the time derivative of average temperature against time (heating rate). The sudden decrease in the heating rate occurs at about 300 s. In contrast, PCM melting begins earlier, after a few seconds in titanium, as well as in steel, stainless steel, and Inconel structures. Indeed, Fig. 3d shows a rapid decrease in the heating rate and Fig. 3b shows that the liquid fraction of palmitic acid within these structures starts to increase very early. However, the heating rate for these metals remains at a high level when compared to silver, copper and aluminium. As a result, the average temperature for the latter three materials is comparatively lower than that associated with titanium, steel, stainless steel and Inconel after 800 s. This observation is strongly corroborated by the data presented in Fig. 3e, wherein the rate of liquid PCM fraction in silver, aluminium, and copper structures consistently surpasses that of the other metal structures. A similar outcome is evident in Fig. 3c, which portrays the average temperature of the solid structure over time. This observation aligns with the previously mentioned trend, as structures composed of silver, aluminium, and copper exhibit a faster rate of temperature increase than the other metals (Fig. 3f). As the average temperature is higher than with the other materials, the structure ensures a faster melting process.

The superior performance of silver, copper, and aluminium in achieving a more rapid average structure temperature ascent is further substantiated through a comparative analysis of their diffusivity, as detailed in Table 3. This enhanced heating rate is attributed to the higher thermal diffusivity of silver, aluminium, and copper when compared to steel, stainless steel, titanium, and Inconel structures. Figs. 4a & 4b show the temperature field in the steel and copper structures respectively after 10 min of heating. The scale of temperature has been chosen so that the minimum temperature is the melting temperature. Therefore, for the steel structure, the temperature of the deep blue part is too low for the surrounding PCM to melt, while the lower part of the structure is very hot. In contrast, for the copper structure, the temperature field is more homogeneous and the whole structure is above the melting temperature. This behaviour is due to the value of the thermal diffusivities. Steel has a low thermal diffusivity, so the heat is not well conducted through the structure, and only the part close to the heated face is hot. We therefore expect the PCM to melt quickly in the lower part and slowly in the upper part. This is consistent with the numerical results presented in Fig. 3b, which show that the PCM begins to melt

Table 2
Properties of the metals and PCMs involved in the simulation [13,85–89].

Properties	T_m (°C)	$\Delta H_f\left(kJ.kg^{-1}\right)$	$\rho\left(kg.m^{-3}\right)$	$c_p\left(J.kg^{-1}.K^{-1}\right)$	$\lambda\left(W.m^{-1}.K^{-1}\right)$	$\mu \times 10^6$(Pa.s)
Steel	1410.0	250.00	7900	500	15	
Silver	961.9	104.73	10,500	235	430	
Aluminium	660.0	388.00	2700	900	237	
Inconel	1264.6	196.85	8190	435	11	
Stainless steel	1400.0	260.00	8030	500	14	
Copper	1083.0	204.00	8950	380	400	
Titanium	1725.0	390.00	4500	520	20	
Solid palmitic acid	62.2	211.85	989.6	$0.29647T^2 - 163.71T + 24290.7$	0.22	
Liquid palmitic acid			$-0.7349(T - 273.15) + 907.54$	2390	0.16	$4.381exp\frac{2488.8}{T}$
Solid myristic acid	53.8	195.44	1000.2	$0.3179T^2 - 171.91T + 24969.3$	0.25	
Liquid myristic acid			$-0.7148(T - 273.15) + 912.02$	2360	0.2	$4.173exp\frac{2401.7}{T}$
Solid stearic acid	69.4	227.84	1040.9	$0.18773T^2 - 102.94T + 15642.4$	0.26	
Liquid stearic acid			$-0.75879(T - 273.15) + 1119.78$	2180	0.19	$3.482exp\frac{2666.6}{T}$

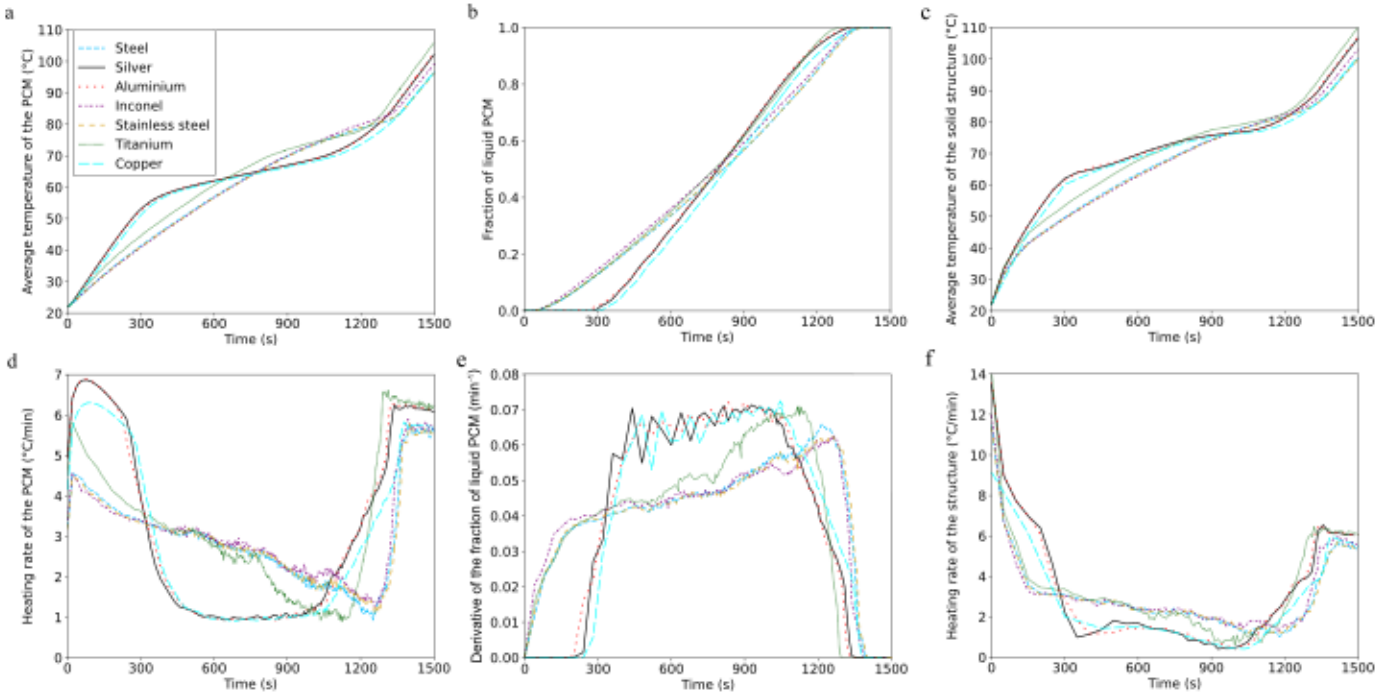

Fig. 3. a) Average temperature of the PCM (palmitic acid) against time. b) Fraction of liquid in the PCM (palmitic acid) volume against time. c) Average temperature of the porous metal architected structure against time. d) Heating rate (time derivative of average temperature) of the PCM against time. e) Rate of the fraction of liquid in the PCM (time derivative of liquid fraction) against time. f) Heating rate of the porous metal architected structure against time.

Table 3
Diffusivity of each metal tested as the material of the architected porous structure in descending order.

Type of metal	Diffusivity ($m^2 \cdot s^{-1}$)
Silver	1.7×10^{-4}
Copper	1.2×10^{-4}
Aluminium	9.8×10^{-5}
Titanium	8.5×10^{-6}
Steel	3.8×10^{-6}
Stainless steel	3.5×10^{-6}
Inconel	3.1×10^{-6}

near the bottom heated face after a few seconds inside the gyroid in steel. Copper has a high thermal diffusivity, so the heat is well conducted, and the temperature gradient in the structure is lower than for steel. We expect the PCM to melt homogeneously throughout the structure and not just near the bottom as with steel. The PCM therefore starts to melt later than in a steel gyroid (Fig. 3b), but more quickly once the melting process starts.

Fig. 5 presents the melting process for both configurations at different times. In particular, it shows the part of the PCM that is still solid. As expected, the melting behaviour is by no means the same depending on the structure material. For steel, the melting interface goes up with time. This pattern is not very efficient as the surface area of this interface is small and the benefit of the triply-periodic gyroid shape is lost. As the lower part is very hot, after 10 min, more PCM is melted with steel than with copper, but the trend is reversed afterwards. For copper, the PCM melts in every part of the porous structure and the melting interface area is therefore larger than with steel. The simulations show that this behaviour is preferable to make the PCM melt faster. It is worth noting that the first behaviour is shared by the other porous architected structures made of stainless steel, titanium, and Inconel, while the second one is shared by structures made of silver and aluminium.

The simulation results presented in Fig. 6a and b track the average temperature and heating rate of the lower heated face of the architected

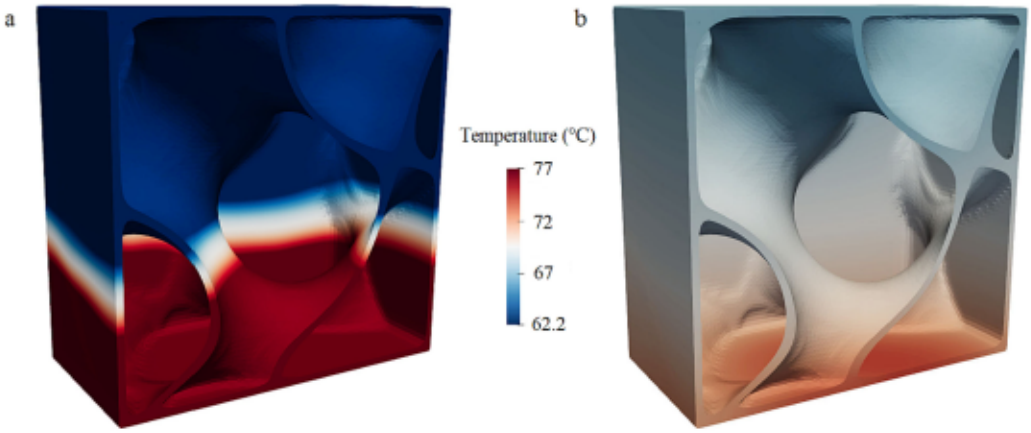

Fig. 4. Temperature of the structure impregnated with PCM after 10 min of heating using a) steel, b) copper.

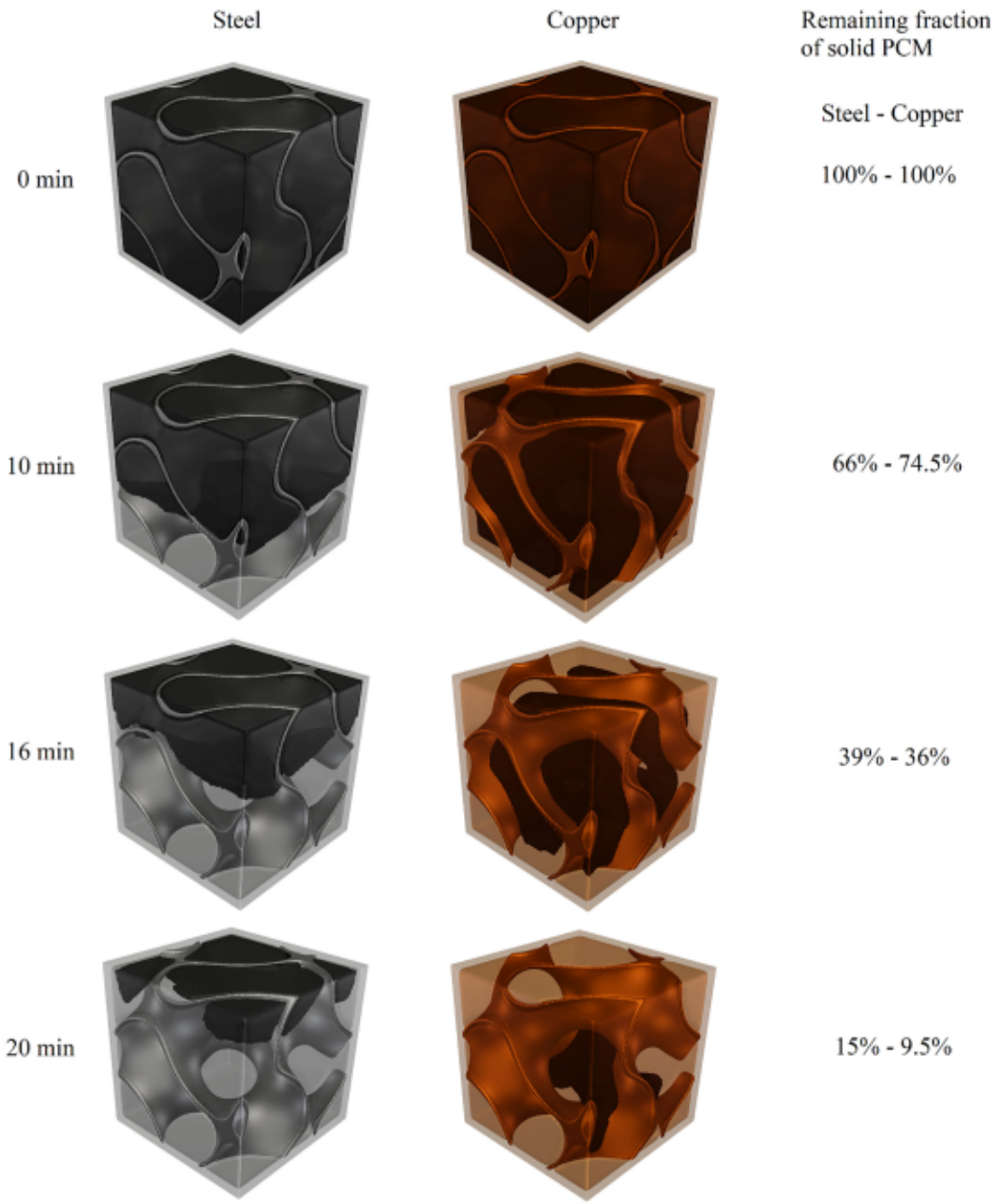

Fig. 5. Steel and copper structures impregnated with PCM. The solid part of the PCM is shown at the beginning, after 10, 16 and 20 min of heating. The remaining fraction of solid PCM is given for both configurations at each time.

structure.

Fig. 6a reveals that the lower face of the titanium, steel, stainless steel, and Inconel structures registers notably higher temperatures when compared to the silver, aluminium, and copper structures. This disparity arises from the slowest transfer of generated heat from the heat source to the impregnated PCM due to the lower thermal diffusivity and greater thermal resistance inherent in metals such as steel (Fig. 4a). Conversely, the lower face of the copper structure exhibits a lower average temperature due to its superior thermal diffusivity (Table 3), which is consistent with Fig. 4b. This difference in thermal diffusivity is also reflected in Fig. 6b, where the heating rate of the lower face of the titanium, steel, stainless steel, and Inconel structures is significantly higher at the outset of the process. This discrepancy arises from these metals transferring heat to the impregnated PCM at a slower rate compared to copper, aluminium, and silver, resulting in a higher heating rate at the bottom of the structures.

4.2. *Influence of the PCM*

As indicated by the simulation results presented in the previous section, among the materials under consideration, copper, aluminium, and silver have demonstrated superior performance for potential use in the fabrication of porous structures. This advantage is attributed to their greater thermal diffusivity. Consequently, among the three viable metals (copper, silver, and aluminium), copper has been chosen for further simulation, wherein various PCMs are employed to investigate PCM/metal porous structures. This choice is based on considerations of cost-effectiveness and thermomechanical stability. Silver is relatively expensive [90], and both aluminium and silver present high thermal expansion which could lead to undesired deformation [91]. Furthermore, aluminium always has a layer of aluminium oxide on its surface, making its densification through additive manufacturing techniques challenging.

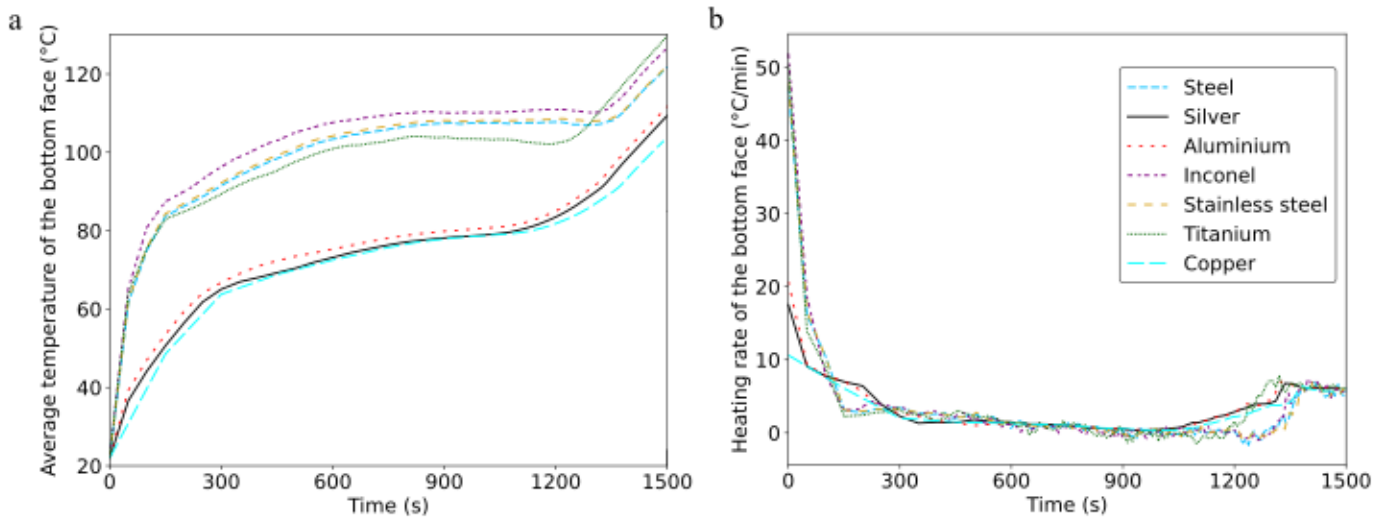

Fig. 6. a) Average temperature of the bottom face of the porous architected structure against time. b) Heating rate of the average temperature of the bottom face of the porous architected structure against time.

The selected PCMs for this study include palmitic acid, myristic acid, and stearic acid. Fig. 7 provides a visual representation of the average temperature and heat rate profiles for both the PCMs and the solid structure.

Fig. 7a provides an overview of the average temperature profiles of the PCMs over time. Notably, it illustrates that the melting process of

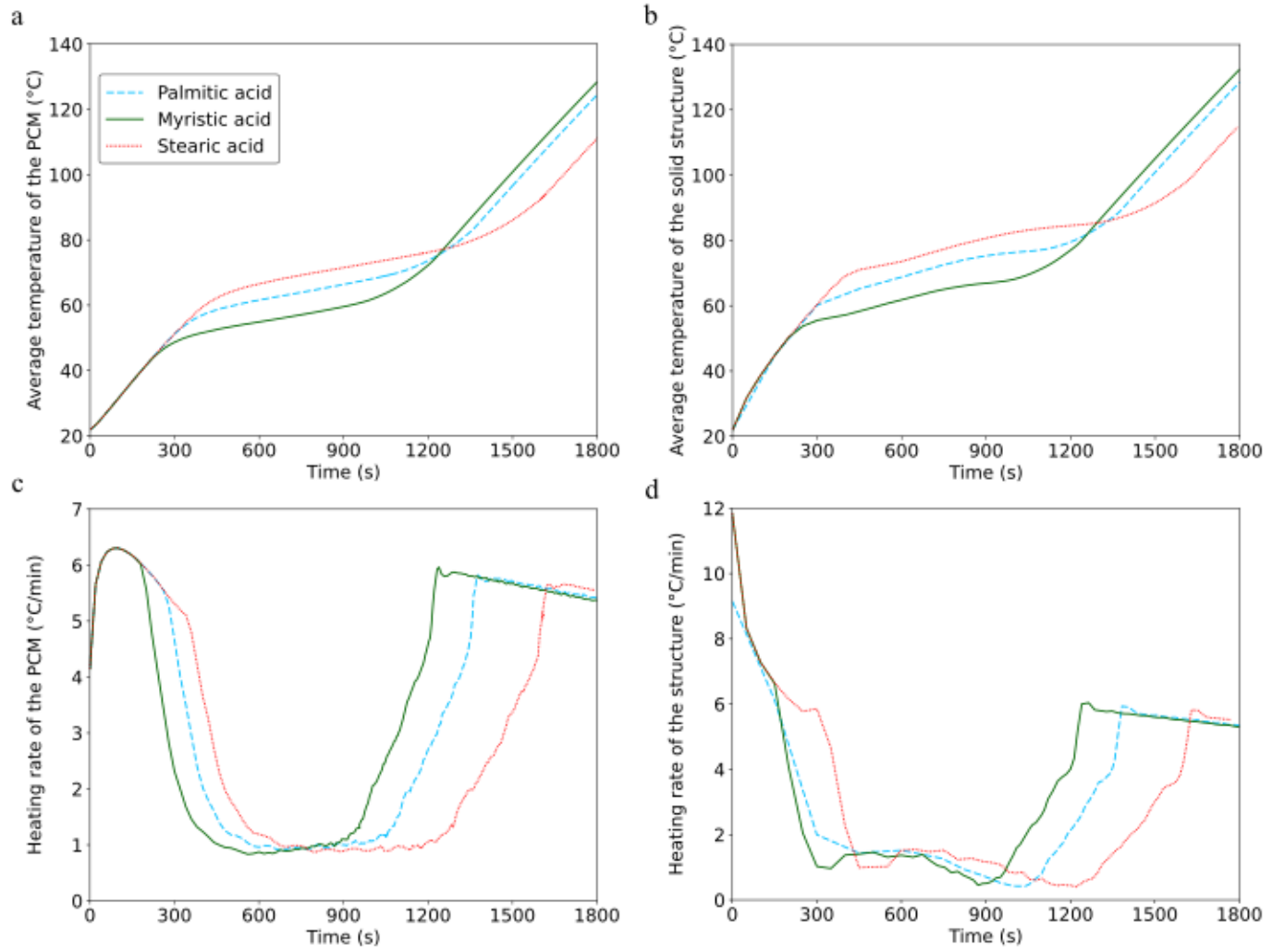

Fig. 7. a) Average temperature against time. b) Average temperature of the porous copper architected structure against time. c) Heating rate (time derivative of average temperature) against time. d) Heating rate of the porous copper architected structure against time.

myristic acid begins earlier than that of palmitic acid and stearic acid, occurring before 300 s. This behaviour is attributed to myristic acid's lower melting temperature in comparison to the other two PCMs. Additionally, the higher latent heat content of stearic acid leads to a prolonged melting process in comparison to palmitic acid and myristic acid. In Fig. 7b, the average temperature of the copper structure containing myristic acid demonstrates a rapid increase within the initial 300 s, indicative of the sensible heat region of the PCM. Subsequently, after 300 s, myristic acid begins to melt, and due to its latent heat, the solid structure experiences a more gradual temperature rise. This trend persists until approximately 1200 s when myristic acid is fully melted, and the temperature of the solid structure begins to increase at a faster rate. A similar progression is observed for palmitic acid and stearic acid. Fig. 7c and d provide insights into the heating rate of both the PCMs and the solid structure, respectively. Notably, the heating rate of myristic acid begins to decrease earlier than that of palmitic acid and stearic acid, primarily due to its lower melting temperature. However, while the PCMs are still in their solid state, their heating rates decrease at a nearly identical rate. Furthermore, when the PCMs are fully melted, it is evident that their heat rates increase at a nearly identical rate as well. The same principle is applicable to the heating rate of the solid structure, as illustrated in Fig. 7d. The heating rate of the solid structure remains relatively stable during the solid-liquid phase transition of the PCMs. This stability arises from the fact that the heat supplied by the heat source is primarily used to increase the enthalpy of the PCMs, causing them to melt. For PCMs such as stearic acid, which has a higher latent heat of fusion than myristic acid, a longer time is required for complete melting. Consequently, during this phase, the heating rate of the solid structure maintains its stability. The variation in the latent heat of fusion of PCMs has a direct impact on both the liquid fraction and the rate of liquid fraction change, as depicted in Fig. 8a and b, respectively.

The lower melting temperature of myristic acid appears clearly in Fig. 8a, where its melting process initiates before the other two PCMs. Additionally, due to myristic acid's lower latent heat compared to palmitic acid and stearic acid, it achieves a higher rate of liquid fraction change, as shown in Fig. 8b. In the region of the graph where the rate of liquid fraction stabilizes, the generated heat is primarily being used to increase the enthalpy of the PCMs. When the PCMs are fully melted, the rate of liquid fraction change drops significantly, signifying the completion of the phase change process.

The average temperature and heating rate of the copper porous structure at bottom face against time are monitored in the simulations and illustrated in Fig. 9a and b, respectively.

Impregnating myristic acid into the copper porous structure leads to a noticeable effect. After approximately 300 s, there is a discernible slowing down in the rate of temperature increase at the bottom face. This phenomenon indicates that the PCM is absorbing heat to transfer from solid phase to liquid and thereby mitigating the rapid rise in temperature at the bottom face, a trend that is also evident in Fig. 9b. After about 1200 s, when myristic acid has completely melted, the temperature at the bottom face of copper starts to increase at a higher constant rate. Similar principles apply to palmitic acid and stearic acid, but at higher temperatures than for myristic acid. The difference between the latent heats of fusion of these PCMs causes the rate of heating at the bottom face to slow down for different durations. Impregnated stearic acid, with its higher latent heat of fusion in comparison to palmitic acid and myristic acid, experiences a longer duration of this slowing effect.

Our study underscores the pivotal role of PCM selection in shaping the thermal behaviour of electronic devices. The choice of PCM has proven to be a critical factor in addressing a wide range of heat management challenges in modern electronic devices. Specifically, myristic acid, distinguished by its lower melting point and higher latent heat values (326.98 K and 195.44 $J.g^{-1}$, respectively) compared to palmitic acid and stearic acid, displays an early onset of the melting process. Given that mobile phone CPUs typically exhibit lower power consumption and heat flux compared to those in laptops and data centres, the unique characteristics of myristic acid position it as an ideal candidate for effectively managing heat in compact, heat-sensitive devices like mobile phones. In the context of thermal management for CPUs in laptops and data centres, where higher power consumption and heat flux are anticipated, we should select palmitic acid, characterized by a melting temperature of 335.35 K and a latent heat of fusion of 211.85 $J.g^{-1}$, as well as stearic acid, which possesses a melting temperature of 342.53 K and a latent heat of fusion of 227.84 $J.g^{-1}$, in our simulations. These PCM choices align with the increased thermal demands of such applications, emphasizing the significance of tailored PCM selection based on specific thermal management requirements.

5. Conclusion

In this comprehensive study, we conducted meticulous simulations to unravel the intricate interplay between porous architectural structures, varying metal compositions encompassing silver, copper, aluminium, titanium, steel, stainless steel, and Inconel, and the incorporation of palmitic acid, myristic acid, and stearic acid as PCMs. Our

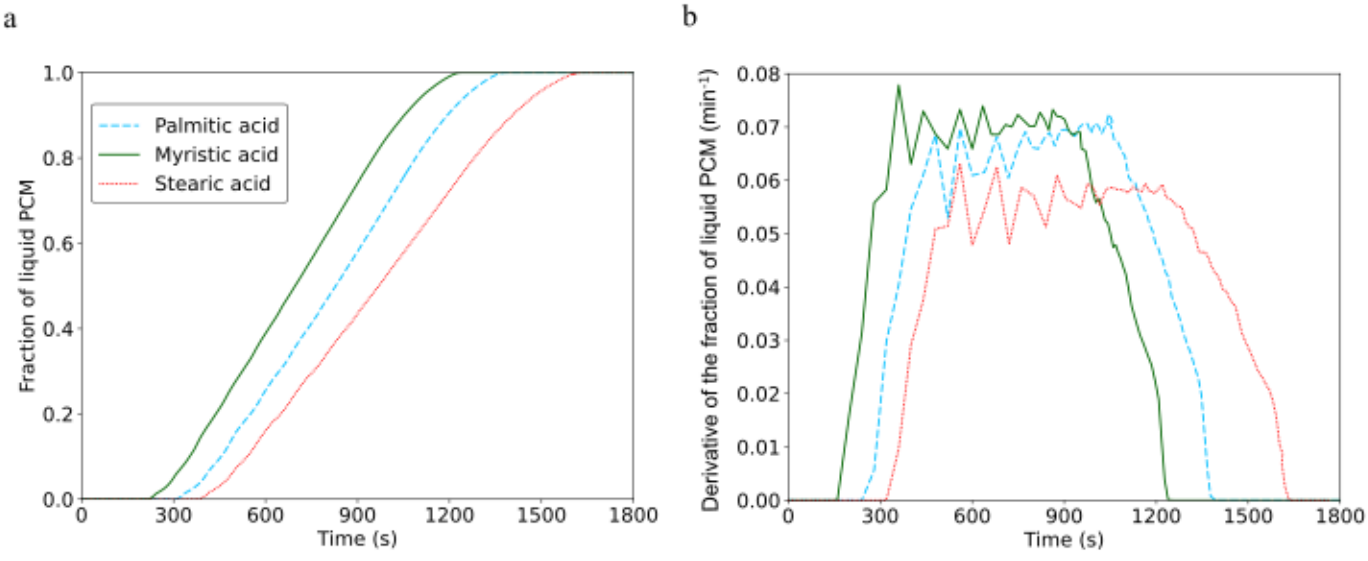

Fig. 8. a) Fraction of liquid in the PCM volume against time. b) Rate of the fraction of liquid in the PCM (time derivative of liquid fraction) against time.

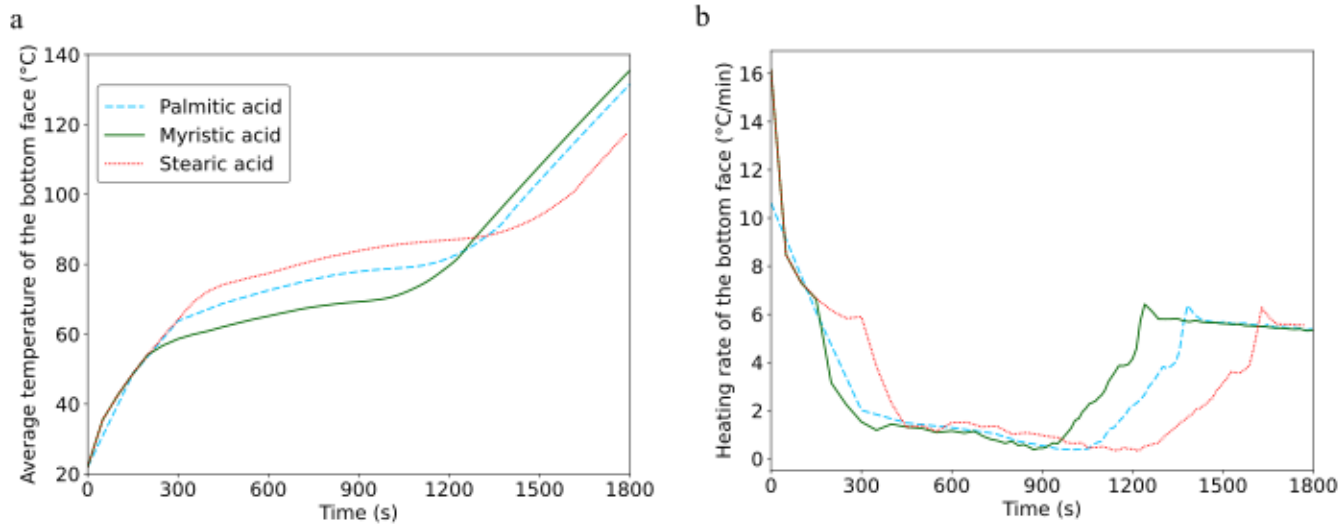

Fig. 9. a) Average temperature of the bottom face of the porous copper architected structure against time. b) Heating rate of the average temperature of the bottom face of the porous copper architected structure against time.

investigations focused on the dynamic relationship between time and temperature within these innovative PCM/porous metal configurations, aiming to assess their efficacy in heat dissipation, a topic of paramount importance in modern thermal management.

The results yielded pivotal insights with far-reaching implications:

(i) Metal influence on thermal performance: Significantly, our findings underscored the pivotal role of metal selection in dictating the performance of these structures. Notably, silver, copper, and aluminium emerged as superior candidates, demonstrating an unparalleled capacity for swift temperature elevation. This characteristic, attributed to their high thermal diffusivity, signifies their potential as frontrunners in advanced thermal management solutions. However, other metals, including titanium, steel, stainless steel, and Inconel, offered valuable insights into alternative applications and scenarios.

(ii) PCM selection and its dynamic impact: The choice of PCM in these simulations proved to be a pivotal determinant of thermal behaviour. Myristic acid, characterized by a lower melting temperature and latent heat, exhibited an early onset of the melting process. This characteristic positions myristic acid as a promising candidate for addressing the intricate thermal management challenges associated with compact, heat-sensitive devices such as mobile phones. In contrast, palmitic acid and stearic acid, with their higher melting temperatures, offer compelling potential for applications demanding elevated thermal thresholds, such as laptops and data centres. These nuanced considerations underscore the strategic versatility of PCMs in catering to diverse thermal management needs.

(iii) Liquid fraction rate dynamics: Our investigations emphasized the instrumental role of metals with elevated thermal diffusivity, expediting the transition to a higher liquid fraction within the PCM. This underscores the necessity of judiciously considering both metal and PCM attributes in TMS.

(iv) Nuanced understanding of heating dynamics: A comprehensive understanding of heating rate dynamics is a critical outcome of this study. Initially, the heating rate of the PCM experiences a surge, driven by the heightened thermal diffusivity of the metals employed in the simulations. This initial surge is followed by a stabilization phase, indicating the PCM's absorption of heat during the crucial melting process. These observations highlight the intricate interplay between the thermal properties of metals and PCMs in heat dissipation systems, shedding light on opportunities for optimizing thermal management strategies.

In summation, our study stands as a significant contribution to the evolving landscape of thermal management, poised to impact a broad spectrum of disciplines reliant on efficient heat dissipation. The discerning selection of metals, informed by their thermal properties, in conjunction with strategically chosen PCMs, represents a critical avenue for advancing the efficacy of porous architectural structures.

We anticipate that our findings will serve as a catalyst for further exploration and innovation in the realm of thermal management, with potential applications extending to electronic devices. The combination of advanced materials, architected structural design, and dynamic thermal behaviours has the potential to advance the field of modern TMS.

CRediT authorship contribution statement

F. Salmon: Writing – original draft. **H. Benisi Ghadim:** Writing – original draft. **A. Godin:** Writing – review & editing. **D. Haillot:** Writing – review & editing. **A. Veillere:** Writing – review & editing. **D. Lacanette:** Writing – review & editing. **M. Duquesne:** Writing – review & editing.

Declaration of competing interest

The authors declare that they have no known competing financial interests or personal relationships that could have appeared to influence the work reported in this paper.

Data availability

No data was used for the research described in the article.

Acknowledgement

We would like to express our gratitude the Laboratory for Energy and Environmental Efficiency of Envelopes and Cities, 4ev Lab, Joint Laboratory between EDF R&D, CNRS and LaSIE. We also would like to thank CNRS for promoting the École de Technologie Supérieure (ÉTS), LaSIE exchanges in the framework of the IEA PHABUL-E project.

References

[1] Mathew J, Krishnan S. A review on transient thermal management of electronic devices. J Electron Packag 2022;144(1).
[2] Smoyer JL, Norris PM. Brief historical perspective in thermal management and the shift toward management at the nanoscale. Heat Transf Eng 2019;40(3–4):269–82.

[3] Bar-Cohen A, Wang P. Thermal management of on-chip hot spot. J Heat Transfer 2012;134(5).
[4] Shamberger PJ, Bruno NM. Review of metallic phase change materials for high heat flux transient thermal management applications. Appl Energy 2020;258:113955.
[5] Khattak Z, Ali HM. Air cooled heat sink geometries subjected to forced flow: a critical review. Int J Heat Mass Transf 2019;130:141–61.
[6] Wang C, Huang X-J, Vafai K. Analysis of hotspots and cooling strategy for multilayer three-dimensional integrated circuits. Appl Therm Eng 2021;186:116336.
[7] Nazir H, et al. Recent developments in phase change materials for energy storage applications: a review. Int J Heat Mass Transf 2019;129:491–523.
[8] Sharma A, et al. Review on thermal energy storage with phase change materials and applications. Renew Sustain Energy Rev 2009;13(2):318–45.
[9] Al-Omari SAB, et al. A heat sink integrating fins within high thermal conductivity phase change material to cool high heat-flux heat sources. Int J Therm Sci 2022;172:107190.
[10] Attaran M. The rise of 3-D printing: the advantages of additive manufacturing over traditional manufacturing. Bus Horiz 2017;60(5):677–88.
[11] Gao W, et al. The status, challenges, and future of additive manufacturing in engineering. Comp Aid Design 2015;69:65–89.
[12] Qureshi ZA, et al. Thermal characterization of 3D-printed lattices based on triply periodic minimal surfaces embedded with organic phase change material. Case Stud Therm Eng 2021;27:101315.
[13] Salmon F, et al. 3D fluid–structure simulation of innovative composites for the design and thermal management of electronic devices. Energ Conver Manage 2023;280:116824.
[14] Previati G, Mastinu G, Gobbi M. Thermal Management of Electrified Vehicles—a Review. Energies 2022;15(4):1326.
[15] Jones-Jackson S, Rodriguez R, Emadi A. Jet impingement cooling in power electronics for electrified automotive transportation: current status and future trends. IEEE Trans Power Electron 2021;36(9):10420–35.
[16] Abramushkina E, et al. A thorough review of cooling concepts and thermal management techniques for automotive WBG inverters: topology, technology and integration level. Energies 2021;14(16):4981.
[17] Lajunen A, Yang Y, Emadi A. Recent developments in thermal management of electrified powertrains. IEEE Trans Veh Technol 2018;67(12):11486–99.
[18] López I, et al. Next generation electric drives for HEV/EV propulsion systems: technology, trends and challenges. Renew Sustain Energy Rev 2019;114:109336.
[19] Jafari S, Nikolaidis T. Thermal management systems for civil aircraft engines: review, challenges and exploring the future. Appl Sci 2018;8(11):2044.
[20] Wileman A, Aslam S, Perinpanayagam S. A road map for reliable power electronics for more electric aircraft. Progr Aerospace Sci 2021;127:100739.
[21] Jixiang W, et al. Recent active thermal management technologies for the development of energy-optimized aerospace vehicles in China. Chin J Aeronaut 2021;34(2):1–27.
[22] Pal D, Severson M. Liquid cooled system for aircraft power electronics cooling. In: 2017 16th IEEE Intersociety Conference on Thermal and Thermomechanical Phenomena in Electronic Systems (ITherm). IEEE; 2017.
[23] Ladeinde F, et al. Experimental measurements and mathematical modeling of cold plate for aviation thermal management. Int J Heat Mass Transf 2022;191:122810.
[24] Raske N, et al. Thermal Management for Electrification in aircraft engines: Optimization of coolant system. In Turbo expo: Power for land, sea, and air. American Society of Mechanical Engineers; 2022.
[25] Tang H, et al. Review of applications and developments of ultra-thin micro heat pipes for electronic cooling. Appl Energy 2018;223:383–400.
[26] gsmarena.com. https://www.gsmarena.com/testing_the_snapdragon_8_gen_1_plus-review-2426p2.php#:~:text=The%20CPU%20performance%20is%20better,watts%20for%20the%20standard%20one; 2022.
[27] Zhou W, et al. Effect of the passage area ratio of liquid to vapor on an ultra-thin flattened heat pipe. Appl Therm Eng 2019;162:114215.
[28] Li J, et al. Mechanism of a microscale flat plate heat pipe with extremely high nominal thermal conductivity for cooling high-end smartphone chips. Energ Conver Manage 2019;201:112202.
[29] Domiciano KG, et al. Thin diffusion bonded flat loop heat pipes for electronics: fabrication, modelling and testing. Energ Conver Manage 2022;255:115329.
[30] Sun Y, et al. Ultrathin flexible heat pipes with Microsorum fortunei structural-like wick for cooling flexible electronic devices. Int J Heat Mass Transf 2023;202:123743.
[31] Zhou G, Li J, Lv L. An ultra-thin miniature loop heat pipe cooler for mobile electronics. Appl Therm Eng 2016;109:514–23.
[32] Shioga T, Mizuno Y, Nagano H. Operating characteristics of a new ultra-thin loop heat pipe. Int J Heat Mass Transf 2020;151:119436.
[33] Chen A, et al. Design, fabrication and thermal performance of a novel ultra-thin loop heat pipe with printed wick structure for mobile electronics cooling. Appl Therm Eng 2022;200:117683.
[34] Chen Z, et al. Design, fabrication and thermal performance of a novel ultra-thin vapour chamber for cooling electronic devices. Energ Conver Manage 2019;187:221–31.
[35] Huang G, et al. A new ultra-thin vapor chamber with composite wick for thin electronic products. Int J Therm Sci 2021;170:107145.
[36] Soni P, et al. A passive thermal energy storage system for laptop cooling using phase change material. 2019.
[37] Sponagle B, Groulx D, White MA. Experimental evaluation of a latent heat storage module with a heat spreader for thermal management of a tablet computer. Appl Sci 2021;11(9):3983.
[38] Intel.ca. 2022.
[39] Zhao Y-N, et al. A new way of supercritical startup of a cryogenic loop heat pipe. Int J Heat Mass Transf 2019;145:118793.
[40] Tian W, et al. Experimental investigation of a miniature loop heat pipe with eccentric evaporator for cooling electronics. Appl Therm Eng 2019;159:113982.
[41] Singh R, et al. Thin thermal management modules using flattened heat pipes and piezoelectric fans for electronic devices. Front Heat Mass Transf (FHMT) 2021:17.
[42] Lim H, et al. Thermal performance of a boiling-driven heat spreader using passive flow control. Case Stud Therm Eng 2023;41:102604.
[43] Wang M, Cui W, Hou Y. Thermal spreading resistance of grooved vapor chamber heat spreader. Appl Therm Eng 2019;153:361–8.
[44] Ding J, et al. Experimental investigation and application analysis on an integrated system of free cooling and heat recovery for data centers. Int J Refrigerat 2022;136:142–51.
[45] Xue ZH, Qu W, Xie MH. High performance loop heat pipe with flat evaporator for energy-saving cooling systems of supercomputers. J Heat Transfer 2020;142(3).
[46] Nadjahi C, Louahlia H, Lemasson S. A review of thermal management and innovative cooling strategies for data center. Sustain Comput Inform Syst 2018;19:14–28.
[47] Zhou H, et al. Combining looped heat pipe and thermoelectric generator module to pursue data center servers with possible power usage effectiveness less than 1. Appl Energy 2023;332:120539.
[48] Li J, et al. A new cooling strategy for edge computing servers using compact looped heat pipe. Appl Therm Eng 2021;187:116599.
[49] Chainer TJ, et al. Improving data center energy efficiency with advanced thermal management. IEEE Trans Compon Packag Manuf Technol 2017;7(8):1228–39.
[50] Cataldo F, et al. Novel pulsating heat pipe for high density power data centres: performance and flow regime analysis. In: 2021 20th IEEE Intersociety Conference on Thermal and Thermomechanical Phenomena in Electronic Systems (iTherm). IEEE; 2021.
[51] Bianco V, De Rosa M, Vafai K. Phase-change materials for thermal management of electronic devices. Appl Therm Eng 2022;214:118839.
[52] Xiao C, et al. Custom design of solid–solid phase change material with ultra-high thermal stability for battery thermal management. J Mater Chem A 2020;8(29):14624–33.
[53] Qureshi ZA, et al. Using triply periodic minimal surfaces (TPMS)-based metal foams structures as skeleton for metal-foam-PCM composites for thermal energy storage and energy management applications. Int Commun Heat Mass Transf 2021;124:105265.
[54] Al-Ketan O, et al. Forced convection computational fluid dynamics analysis of architected and three-dimensional printable heat sinks based on triply periodic minimal surfaces. J Therm Sci Eng Appl 2021;13(2):021010.
[55] Armstrong M, Mehrabi H, Naveed N. An overview of modern metal additive manufacturing technology. J Manufact Proc 2022;84:1001–29.
[56] ISO, A. ISO/ASTM 52900: 2015 additive manufacturing–general principles–terminology. ASTM F2792-10e11; 2015. p. 1–19.
[57] Bandyopadhyay A, Zhang Y, Bose S. Recent developments in metal additive manufacturing. Curr Opin Chem Eng 2020;28:96–104.
[58] Blakey-Milner B, et al. Metal additive manufacturing in aerospace: a review. Mater Design 2021;209:110008.
[59] Gonzalez-Gutierrez J, et al. Additive manufacturing of metallic and ceramic components by the material extrusion of highly-filled polymers: a review and future perspectives. Materials 2018;11(5):840.
[60] Mirzababaei S, Pasebani S. A review on binder jet additive manufacturing of 316L stainless steel. J Manufact Mater Proc 2019;3(3):82.
[61] Atapour M, et al. Corrosion of binder jetting additively manufactured 316L stainless steel of different surface finish. J Electrochem Soc 2020;167(13):131503.
[62] Vafadar A, et al. Advances in metal additive manufacturing: a review of common processes, industrial applications, and current challenges. Appl Sci 2021;11(3):1213.
[63] Kaur I, Singh P. State-of-the-art in heat exchanger additive manufacturing. Int J Heat Mass Transf 2021;178:121600.
[64] Dhinesh SK, et al. Recent trends in additive manufacturing of electronics devices. Mater Today Proc 2022;66:928–41.
[65] Selema A, Ibrahim MN, Sergeant P. Metal additive manufacturing for electrical machines: technology review and latest advancements. Energies 2022;15(3):1076.
[66] Maleki E, et al. Surface post-treatments for metal additive manufacturing: Progress, challenges, and opportunities. Addit Manuf 2021;37:101619.
[67] Durgam S, Ghodake B, Mohite S. Numerical investigation on heat sink material for temperature control of electronics. In: Journal of physics: Conference series. IOP Publishing; 2022.
[68] Muhammad A, et al. Comparison of pressure drop and heat transfer performance for liquid metal cooled mini-channel with different coolants and heat sink materials. J Therm Analys Calorim 2020;141:289–300.
[69] Siahchehrehghadikolaei S, et al. A CFD modeling of CPU cooling by eco-friendly nanofluid and fin heat sink passive cooling techniques. Adv Powder Technol 2022;33(11):103813.
[70] Zhang X, et al. An additively manufactured metallic manifold-microchannel heat exchanger for high temperature applications. Appl Therm Eng 2018;143:899–908.
[71] Chu K, et al. Thermal properties of graphene/metal composites with aligned graphene. Mater Design 2018;140:85–94.
[72] Rojo G, Darabi J. Copper-carbon nanotube micropillars for passive thermal management of high heat flux electronic devices. In: Heat transfer summer conference. American Society of Mechanical Engineers; 2020.
[73] Nekahi S, et al. A numerical approach to the heat transfer and thermal stress in a gas turbine stator blade made of HfB2. Ceram Int 2019;45(18, Part A):24060–9.

[74] Vajdi M, et al. Role of graphene nano-platelets on thermal conductivity and microstructure of TiB2–SiC ceramics. Ceram Int 2020;46(13):21775–83.
[75] Belmonte M, et al. Heat dissipation in 3D printed cellular aluminum nitride structures. J Eur Ceram Soc 2021;41(4):2407–14.
[76] Sarowar MT. Numerical analysis of a liquid metal cooled mini channel heat sink with five different ceramic substrates. Ceram Int 2021;47(1):214–25.
[77] Cao Y, et al. Role of beryllium oxide on the thermal efficiency of microchannel heat exchanger with an optimum fin structure. Ceram Int 2022;48(7):9973–86.
[78] Sarowar MT. Performance comparison of microchannel heat sink using boron-based ceramic materials. Adv Mat Res 2021;1163:73–88.
[79] Markandeyulu T, Devanuri JK, Kumar K. On the suitability of phase change material (PCM) for thermal management of electronic components. Indian J Sci Technol 2016;9(S1):1–4.
[80] Sharma R, et al. Developments in organic solid–liquid phase change materials and their applications in thermal energy storage. Energ Conver Manage 2015;95:193–228.
[81] Magendran SS, et al. Synthesis of organic phase change materials (PCM) for energy storage applications: a review. Nano-structures Nano-objects 2019;20:100399.
[82] Alva G, et al. Thermal energy storage materials and systems for solar energy applications. Renew Sustain Energy Rev 2017;68:693–706.
[83] Da Cunha JP, Eames P. Thermal energy storage for low and medium temperature applications using phase change materials–a review. Appl Energy 2016;177:227–38.
[84] Blanquer SB, et al. Surface curvature in triply-periodic minimal surface architectures as a distinct design parameter in preparing advanced tissue engineering scaffolds. Biofabrication 2017;9(2):025001.
[85] Duquesne M, et al. Characterization of fatty acids as biobased organic materials for latent heat storage. Materials 2021;14(16):4707.
[86] Costa SC, Kenisarin M. A review of metallic materials for latent heat thermal energy storage: Thermophysical properties, applications, and challenges. Renew Sustain Energy Rev 2022;154:111812.
[87] Shahzad A. Thermophysical Properties of complex materials. Rijeka: IntechOpen; 2020.
[88] Thermal Properties of Metals, Conductivity, Thermal Expansion, Specific Heat [cited 2023 08/11/2023]; Available from: https://www.engineersedge.com/properties_of_metals.htm; 2023.
[89] The Engineering ToolBox. Metals - Latent heat of melting [cited 2023 08/11/2023]; Available from: https://www.engineeringtoolbox.com/fusion-heat-metals-d_1266.html; 2008.
[90] Robinson J, Stanford M, Arjunan A. Stable formation of powder bed laser fused 99.9% silver. Mater Today Commun 2020;24:101195.
[91] Nix F, MacNair D. The thermal expansion of pure metals: copper, gold, aluminum, nickel, and iron. Phys Ther Rev 1941;60(8):597.